



# Suppressing subcritical transition in plane Poiseuille flow

Yiyang Sun\* and Maziar S. Hemati†  
*University of Minnesota, Minneapolis, MN, 55455*

**For channel flow at subcritical Reynolds numbers ( $Re < 5772$ ), a laminar-to-turbulent transition can emerge due to a large transient amplification in the kinetic energy of small perturbations, resulting in an increase in drag at the walls. The objectives of the present study are two-fold: (1) to design a feedback control strategy to prevent this subcritical laminar-to-turbulent transition, and (2) to examine the control mechanisms that enable transition suppression. In this paper, we investigate transient energy growth of linear optimal disturbance of plane Poiseuille flow at a subcritical Reynolds number of  $Re = 3000$  using linear analysis and nonlinear simulation. We find that the amplification of the given initial perturbation revealed from linear analysis is suppressed by the presence of the nonlinearity in the direct numerical simulations, with larger initial perturbations being less amplified in general. Moreover, we design linear quadratic optimal controllers to delay transition via wall-normal blowing and suction actuation at the channel walls. We demonstrate that these feedback controllers are capable of reducing transient energy growth in the linear setting. Next, the performance of the same controllers is evaluated for nonlinear flows where a laminar-to-turbulent transition emerges without control. Nonlinear simulations reveal that the controllers can reduce transient energy growth of optimal disturbances and suppress transition. Further, we identify and characterize the underlying physical mechanisms that enable feedback control to suppress and delay laminar-to-turbulent transition. These findings can provide valuable insights and guidance for developing actuation strategies in future investigations.**

## I. Introduction

Channel flow is ubiquitous in engineering applications, and the laminar-turbulent state of the flow is of great practical consequence. In general, since laminar channel flows experience smaller wall friction than turbulent flows, laminar-to-turbulent transition suppression has been a primary objective in flow control studies of channel flows. Extensive studies have been performed to understand characteristics of channel flows [1–5], among which hydrodynamic stability analysis is widely used to examine behaviors of small perturbations around an equilibrium state of the flow. The stability result is often used to determine the critical condition a laminar-to-turbulent transition to arise [6–9]. For plane Poiseuille flows, linear stability analysis identifies a critical Reynolds number of  $Re = 5772$  below which the flow state will remain laminar and small perturbations will decay to zero eventually [7]. However, a laminar-to-turbulent transition in plane Poiseuille flow has been observed in experiments and simulations at Reynolds numbers far smaller than the critical one [10–12]. This phenomenon is caused by a short-time transient amplification of small perturbations before their eventual decay. This so-called transient energy growth results from the non-normality of the linearized perturbation dynamics [13, 14], which can contribute to a laminar-to-turbulent transition observed in plane Poiseuille flow at subcritical Reynolds numbers.

To delay or suppress a transition in plane Poiseuille flow, modern feedback control theory has been investigated and shown to exhibit robustness to uncertainties [15–20]. One approach is to reduce the maximum transient energy by designing feedback control laws using the linear model, as the large energy amplification plays an important role in the transitional process. Recent efforts have sought to account for the nonlinearity effects while designing the feedback controllers by modeling the nonlinearity in the Navier–Stokes equations as feedback uncertainty to the linear dynamical system [21], or in such a way that passivity-based analysis and synthesis can be used for control [22].

Among all the possible disturbances, the optimal disturbance leads to the maximum transient energy growth [9], which has the highest chance to induce a laminar-to-turbulent transition of the flow. The optimal disturbance is usually computed based on the linearized operator [23], though nonlinear notions can also be determined [24]. In the present work, we focus on the initial optimal disturbance computed based on the linear model. The optimal disturbance

\*Postdoctoral Associate, Department of Aerospace Engineering and Mechanics, Member AIAA.

†Assistant Professor, Department of Aerospace Engineering and Mechanics, Senior Member AIAA.

is calculated for the uncontrolled and controlled systems, respectively, because an implementation of controller to the system can possibly induce new optimal disturbance that leads to a larger transient energy growth than for the uncontrolled system [25]. However, this point is rarely discussed in past direct numerical simulation studies [26–28] aiming to evaluate the overall performance of a feedback controller.

In this paper, we first perform linear and nonlinear simulations to study the transient energy growth in plane Poiseuille flows. We investigate nonlinear effects using direct numerical simulations. It is found that the nonlinearity plays a role in suppressing large amplification of kinetic energy, as seen through reductions in amplification with increasing initial kinetic energy. We found that for the oblique and streamwise-wave disturbances, streamwise vortices grow based on the development of coherent vortical structures initiated from the optimal disturbances. The breakdown of these streamwise vortices leads to a laminar-to-turbulent transition. For the spanwise-wave disturbance, high shear is induced between merged and large-scale streamwise vortices where secondary instabilities grow and break the coherent structure to trigger a laminar-to-turbulent transition. We note that these transitional mechanisms are certainly not new, but we will focus on how the actuation in the feedback control alters the undesirable transition process. Linear quadratic controllers are designed to reduce the large transient energy growth experienced in the uncontrolled flows. Actuation is implemented in the form of wall blowing/suction within the nonlinear simulation, which has been shown capable of suppressing or delaying transition. Here, we investigate the control mechanism by which actuation conditions the flow to avoid transition. For the oblique and streamwise-wave disturbances, wall actuation modifies the distribution of high shear present in the flows, which prevents the large transient energy growth associated with the development of coherent structures. For the spanwise-wave disturbance, we will show that wall actuation induces small streamwise vortices near the channel wall, which hinders the growth of merged vortices and further reduces the high shear formed between adjacent streamwise vortical structures. These underlying flow control mechanisms can provide valuable guidance for future actuation strategies.

The paper is organized as follows. Numerical approaches are provided in section II with a linear model for feedback control design and computational setup for direct numerical simulations. In section III, we discuss uncontrolled flows that exhibit transition for various optimal disturbances. The results for controlled flows are also provided in this section with detailed discussions of the control mechanisms. Finally, conclusions are summarized in section IV.

## II. Numerical Approaches

### A. Linearized Navier–Stokes equations and feedback control design

To use modern control theory to design feedback controllers, a state-space representation of the fluid flow problem is required. For plane Poiseuille flow,  $x$ ,  $y$  and  $z$  indicate streamwise, wall-normal and spanwise directions, respectively, and corresponding velocity components are  $\mathbf{u}$ ,  $\mathbf{v}$  and  $\mathbf{w}$ . Time is denoted by  $t$ . We decompose the flow state  $\tilde{\mathbf{q}}$  into base state  $\bar{\mathbf{q}}$  and small perturbation  $\mathbf{q}'$ , where  $\mathbf{q} = [\mathbf{u}, \mathbf{v}, \mathbf{w}, p]^T$  ( $p$  is pressure), and the base state velocity profile is of  $[\bar{\mathbf{u}}, \bar{\mathbf{v}}, \bar{\mathbf{w}}] = [1 - (y/h)^2, 0, 0]$ , where  $h = 1$ , and the center velocity of the base flow is denoted by  $\bar{u}_c$ . The velocity is non-dimensionalized by  $\bar{u}_c$ . The kinetic energy density of perturbation is defined as

$$E = \frac{1}{2V} \int_{vol=V} (\mathbf{u}'^2 + \mathbf{v}'^2 + \mathbf{w}'^2) dvol, \quad (1)$$

where  $V$  is the volume of computational domain.

By substituting the expression of  $\tilde{\mathbf{q}} = \bar{\mathbf{q}} + \mathbf{q}'$  into the Navier–Stokes equations, and assuming that the perturbation is much smaller than the base state in magnitude  $|\mathbf{q}'| \ll |\bar{\mathbf{q}}|$ , we linearize the equations by retaining linear terms and neglecting higher order nonlinear terms. Next, the real-valued perturbation is expressed as Fourier expansion

$$\mathbf{q}'(x, y, z, t) = \mathbf{q}(y, t)e^{i(\alpha x + \beta z)} + \text{complex conjugate}, \quad (2)$$

where  $\mathbf{q}(y, t)$  is amplitude function of the perturbation associated with streamwise wavenumber  $\alpha$  and spanwise wavenumber  $\beta$ . By plugging Eq. (2) into the linearized Navier–Stokes equations, we can reformulate the governing equations into a state-space form

$$\frac{\partial X}{\partial t} = A(\bar{\mathbf{q}}; \alpha, \beta)X, \quad (3)$$

where  $X = [\mathbf{v}', \boldsymbol{\eta}']$ ,  $\mathbf{v}'$  is wall-normal velocity perturbation, and  $\boldsymbol{\eta}'$  is wall-normal vorticity perturbation. Dynamics matrix  $A$  is derived from linearized Navier–Stokes equations which follows the form proposed by Schmid & Henningson

[9]. By choosing real-valued wavenumber pair of  $(\alpha, \beta)$ , we can analyze perturbations associated with various structures. In the present work, we examine optimal disturbances with three different wavenumber pairs —  $(\alpha, \beta) = (1, 0)$ ,  $(0, 2)$  and  $(1, 1)$ . The features of each optimal disturbance will be discussed in the result section III.

In the control design, we introduce actuation in the form of blowing and suction on the upper and lower channel walls. To synthesize this actuation into the dynamical system, we add a control input term  $BU$  to the uncontrolled system (Eq. (3)) to form the system

$$\frac{\partial X_c}{\partial t} = A_c X_c + BU, \quad (4)$$

where the control inputs in  $U = \frac{\partial}{\partial t}[v'_{+h}, v'_{-h}]$  are the rate of change of wall-normal velocity on the upper and lower walls, and  $B$  is the input matrix that maps the influence of control inputs on the system. Due to the no-slip boundary condition ( $v'_{\pm h} = 0$ ) applied on the walls of the uncontrolled flow,  $v'_{\pm h}$  are excluded while forming the flow state  $X$  in Eq. (3). As  $v'_{\pm h}$  are nonzero in the controlled flow, we will append these two variables to the flow state  $X$  to form a new state  $X_c = [X, v'_{+h}, v'_{-h}]^T$ . Analogously, the dynamics matrix  $A$  is modified and denoted by  $A_c$  to account for the new state. More information about the system modeling can be found in the work by McKernan et al. [29].

Based on the state-space model in Eq. (4), linear quadratic regulator (LQR) is designed for use in feedback control. The control objective is to minimize

$$J = \int_0^{\infty} (X^T Q X + U^T R U) dt. \quad (5)$$

Here, subject to the linear dynamics (Eq. 4),  $Q$  and  $R$  are weight matrices. The term  $X^T Q X$  represent kinetic energy density  $E$ , and  $R$  is a diagonal matrix with each element equals  $10^{-6}$  to penalize the control input. The feedback control law is given by  $U = -KX$ , where matrix  $K$  is the state feedback control gain. Given the state matrix  $A_c$ , input matrix  $B$ , weight matrices  $Q$  and  $R$ , the static control gain matrix  $K$  can be calculated by solving an algebraic Riccati equation [30]. The LQR controller is implemented in the direct numerical simulations, as discussed below.

## B. Direct numerical simulation

Two- and three-dimensional direct numerical simulations of plane Poiseuille flow are performed using a spectral code *Channelflow* [31, 32] to solve the incompressible Navier–Stokes equations. A second-order Runge–Kutta temporal scheme is used. As shown in figure 1, the flow between two infinite planes has a base velocity profile of  $[\bar{u}, \bar{v}, \bar{w}] = [1 - (y/h)^2, 0, 0]$  at Reynolds number of  $Re = 3000$ . In the simulations, periodic boundary conditions are assumed in the  $x$ - and  $z$ -directions in which the flow variables are represented by Fourier expansion. In the  $y$ -direction, flow variables (velocity and pressure) are represented by Chebyshev polynomials, and no-slip boundary condition is specified at upper and lower walls for uncontrolled flow. For controlled flow, actuation in form of blowing/suction in  $y$ -direction is introduced on the entire upper and lower walls, which follows the Fourier expansion in the  $x$ - and  $z$ -directions as well. The control strategy illustrated in figure 1 is an example of a case having streamwise wavelike actuation where  $\beta = 0$ . Since the rate of change of wall-normal velocity on walls  $v_{\pm h}$  is updated using the state  $X$  and control gain matrix  $K$  described above in section II.A, the value of  $v_{\pm h}$  can be approximated and implemented by changing  $v_{\pm h}$  as boundary condition at each time step. We also note that as the wavenumber pair of  $(\alpha, \beta)$  is determined while designing the feedback control strategy, the actuation is automatically associated with the same wavenumber pair that characterizes the optimal disturbance.

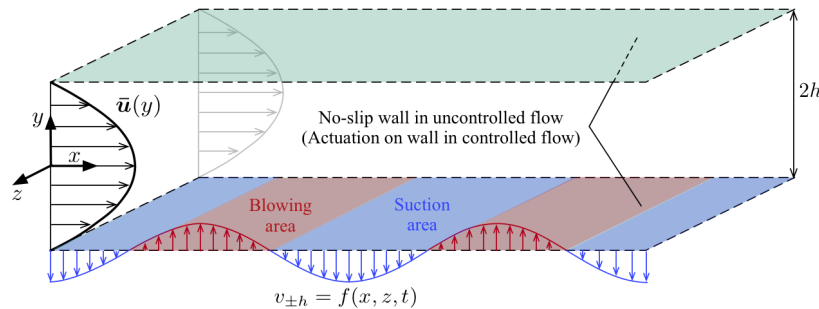


Fig. 1 Schematic of plane Poiseuille flow (not to scale), both with and without wall actuation.

We use a rectangular computational domain of size  $8\pi h \times 2h \times 2\pi h$  in  $x$ -,  $y$ - and  $z$ -directions, respectively. Chebyshev points of  $N = 101$  in the  $y$ -direction is prescribed to discretize the flow field for all the cases. Uniform grids of  $128 \times 64$  are used for the  $x$ - and  $z$ -directions, respectively. Although the cases with either  $\alpha = 0$  or  $\beta = 0$  represent two-dimensional disturbance, the laminar-to-turbulent transition is a three-dimensional flow phenomenon [33] such that a three-dimensional mesh is necessary to resolve the transitional process in the simulations. For both uncontrolled and controlled flows, grid resolution studies with doubled grids in each direction have been performed to ensure accuracy of the results. Moreover, we have also studied the influences of computational domain size on the simulations results. In past studies, the domain size is usually set to fit one wavelength of the wavenumber of interest for each direction. However, as the transition includes large-scale deformation of original perturbation structures, here we selected a relatively larger domain to resolve the flow in order to have a better understanding of the transitional process in this study. The evolution of perturbation before transition happens is not affected by the domain size, but the time that a transition takes place is slightly dependent on the domain size. Once a sufficiently large domain size is determined, the observations among cases are consistent in general regardless of domain size.

For the simulations of both uncontrolled and controlled cases, the initial condition of flow field consists of the base flow  $[\bar{u}, \bar{v}, \bar{w}]$  and a small perturbation  $[u'_0, v'_0, w'_0]$ . The perturbation is the optimal disturbance associated with a wavenumber pair of  $(\alpha, \beta)$ , and its kinetic energy density is denoted by  $E_0$ . The optimal disturbance can lead to a maximum transient energy and it is pre-calculated using the algorithm proposed by Whidborne and Amar [23]. Since the dynamical systems of the uncontrolled and controlled flows are different due to the wall boundary condition, the optimal disturbance is calculated for each system independently to guarantee that we examine the largest transient energy growth in each case. Moreover, a random perturbation is added with kinetic energy density of 1% of  $E_0$  to expedite an emergence of a laminar-to-turbulent transition in the flows but not significantly affect the feature of the optimal disturbance.

### III. Results and Discussions

In this section, transient energy growth of optimal disturbances associated with three wavenumber pairs of  $(\alpha, \beta) = (1, 0), (0, 2)$  and  $(1, 1)$  is investigated using direct numerical simulations for the subcritical plane Poiseuille flow. The required condition for a laminar-to-turbulent transition to appear in a fully nonlinear flow is examined for each case. The flow features that are responsible for the transition is examined. Moreover, we present a feedback control strategy that can successfully suppress or delay the transition, and the underlying physics related to the control mechanisms are discussed.

#### A. Transient energy growth of optimal disturbance

In this section, we start the discussion from the nonlinearity effects on transient energy growth without random perturbation. With only optimal disturbance as initial condition, the Navier–Stokes equations were integrated to obtain the trajectory of kinetic energy density as shown in figure 2. In the linear simulation, the transient energy growth remains identical if normalized by its initial value  $E_0$ , which is denoted by red dots in each subplots. All the optimal disturbances considered in the present work experience large transient energy amplifications in an order of magnitude from  $O(10^1)$  to  $O(10^3)$ , among which the disturbance of streamwise vortices ( $\alpha = 0, \beta = 2$  in figure 2 (b) ) reaches the largest maximum transient energy growth.

In the nonlinear simulations, we integrate the Navier–Stokes equations of full state velocity  $\tilde{u}$  and report the kinetic energy density of perturbations after subtracting the base flow  $\bar{u}$ . As shown in figure 2, when the perturbation is small enough such as  $E_0 \lesssim 10^{-8}$ , nonlinearity effect is negligible that the trajectory of the transient energy growth is identical to that of the linear result. However, when the amplitude of initial disturbance increases, the amplification of kinetic energy density  $E/E_0$  decreases, which suggests that nonlinearity can suppresses large amplification of optimal disturbance. In other words, the presence of nonlinearity competes with the linear non-modal growth, and inhibits the transient energy amplification for sufficiently large  $E_0$ .

Although we have seen transient energy growth in both linear and nonlinear simulations, however, there is no laminar-to-turbulent transition observed, suggesting that the growth of optimal disturbance solely cannot trigger the transition. As discussed in the study by Reddy et al. [33] that random perturbation is required to observe transitions in simulations, which is more resemblant of the practical environment with various disturbance in the flow. Hence, we added amplitude of 1% of  $E_0$  of random perturbation to the flows in which we observed laminar-to-turbulent transitions. Before the transition appears in the flow, the trajectory of transient energy growth is almost identical to the simulation results without random perturbation. We note that the random perturbation added into the flow will quickly decay to zero

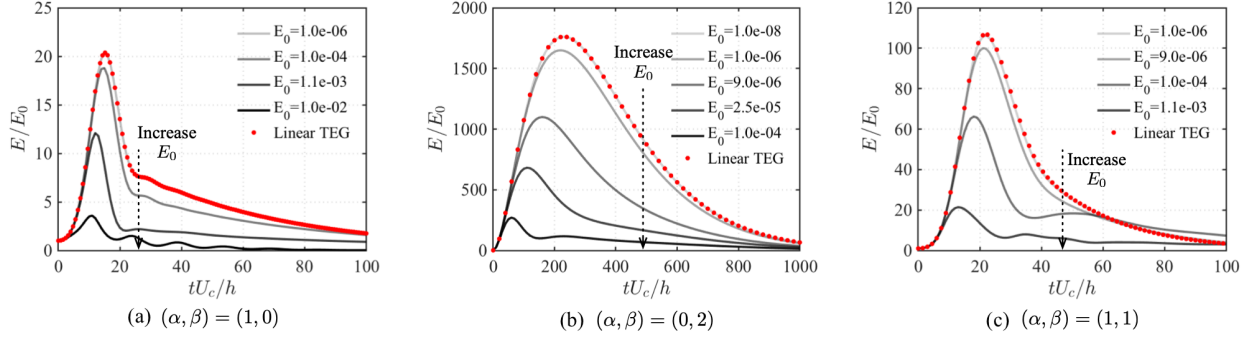


**Fig. 2** Transient energy growth of optimal disturbance with a range of initial kinetic energy density  $E_0$  from linear (red dots) and nonlinear (solid lines) simulations for uncontrolled flows.

without a transitional amplification if the optimal disturbance is not introduced together. Since the transition process of each wavenumber pair follows different routes, we will discuss all the three paths to transition below respectively.

*1. Oblique disturbance  $(\alpha, \beta) = (1, 1)$*

Flow fields of a laminar-to-turbulent transition case with  $(\alpha, \beta) = (1, 1)$  and  $E_0 = 0.5 \times 10^{-4}$  is shown in figure 3. The initial optimal disturbance is in an oblique-wave form and has large value of disturbance near the channel walls. As the disturbance evolves in time, large-scale oblique structures form with size up to half height of the channel. After the transient energy reaches to the maximum value around  $t\bar{u}_c/h = 20$  (can be seen from figure 4), large streamwise vorticity is observed upon the coherent structures and near the channel walls at  $t\bar{u}_c/h = 36$ . Meanwhile, slight spatial variations of the coherent structures appear along the oblique direction. Later at time  $t\bar{u}_c/h = 72$ , streamwise vortices are induced from the oblique coherent structures and grow into streamwise streaks, although the overall transient energy density has started to decay as shown in figure 4. After  $t\bar{u}_c/h = 84$ , these streamwise streaks break into small-scale structures, and a laminar-to-turbulent transition emerges afterwards.

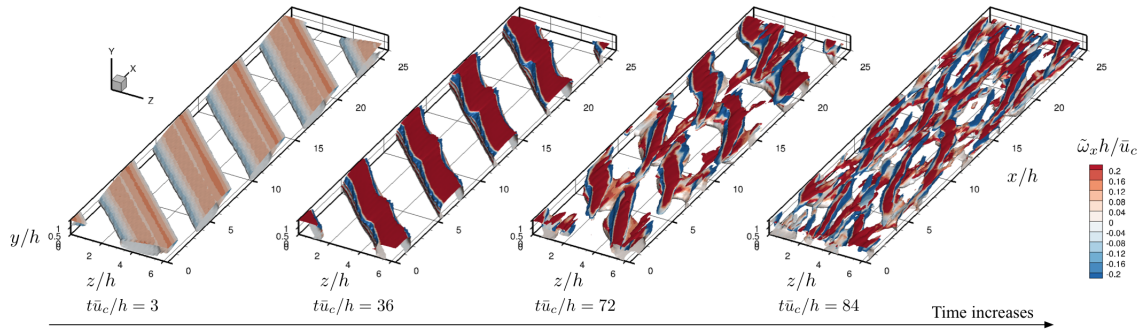


**Fig. 3** Time evolution of flow field to illustrate the laminar-to-turbulent transition process for the case  $(\alpha, \beta) = (1, 1)$ . The flow is initialized by optimal disturbance with kinetic energy density of  $E_0 = 0.5 \times 10^{-4}$ . Iso-surfaces of  $Q$  [34] colored by streamwise vorticity  $\bar{\omega}_x h / \bar{u}_c$  are visualized. Only the upper half domain ( $y \geq 0$ ) is displayed for clarity.

As a sharp increase in friction velocity indicates, the flow has reached a turbulent state. A summary of transitional cases are shown in figure 4 illustrating the features of friction velocity  $u^*$  and corresponding kinetic energy density  $E$  of the flow fields, in which the results of turbulent state has been indicated by dashed lines. Based on the feature of friction velocity, the larger initial disturbance is, the earlier laminar-to-turbulent transition appears. Moreover, large initial disturbance leads to large shear stress in the wall-normal direction near walls. For optimal disturbance with  $E_0 < 0.5 \times 10^{-4}$  denoted by grey lines in figure 4 (right), although the initial disturbance is the most amplified, the induced streamwise vortices (as seen at  $t\bar{u}_c/h = 72$  in figure 3) do not grow significantly, and the disturbance eventually

decays to zero without triggering a laminar-to-turbulent transition. Therefore, a combined effect of initial optimal disturbance and its corresponding amplification determines whether a transition occurs or not. The larger amplitude of disturbance present in the flow has higher chance to trigger a transition to turbulent state, which also indicates that a reduction in transient energy growth has potential to suppress or delay the transition observed in the uncontrolled flow.

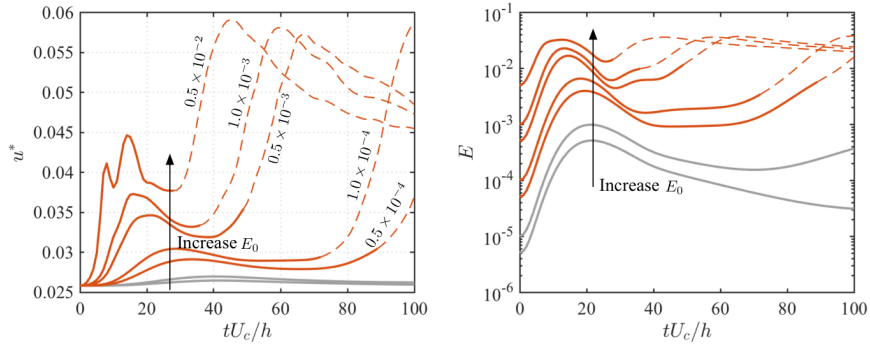


**Fig. 4** Time evolution of friction velocity  $u^*$  (left) and kinetic energy density (right) of case  $(\alpha, \beta) = (1, 1)$  initialized by different amplitudes of optimal disturbance  $E_0$ . Red lines represent transitional cases, and dashed line indicates that the flow is in turbulent state.

## 2. Streamwise-wave disturbance $(\alpha, \beta) = (1, 0)$

The disturbance with wavenumber pair of  $(\alpha, \beta) = (1, 0)$  is the well-known Tollmien-Schlichting waves whose structures are uniform in the spanwise direction. The evolution of the optimal disturbance is shown in figure 5 with  $E_0 = 1.0 \times 10^{-4}$ . As the optimal disturbance grows into large-scale spanwise coherent structures, streamwise vorticity increases near channel walls, especially where the coherent structures reside, as seen in figure 5 at  $t\bar{u}_c/h = 60$ . When the streamwise vorticity is large enough, a  $\Lambda$ -shape structure emerges, splits the spanwise coherent structure and connects to the adjacent spanwise coherent structure in front as seen at  $t\bar{u}_c/h = 108$ . Once the streamwise vortices take place over the spanwise coherent structures stemmed from the optimal disturbance, the break of these vortices leads to a laminar-to-turbulent transition of the flow.

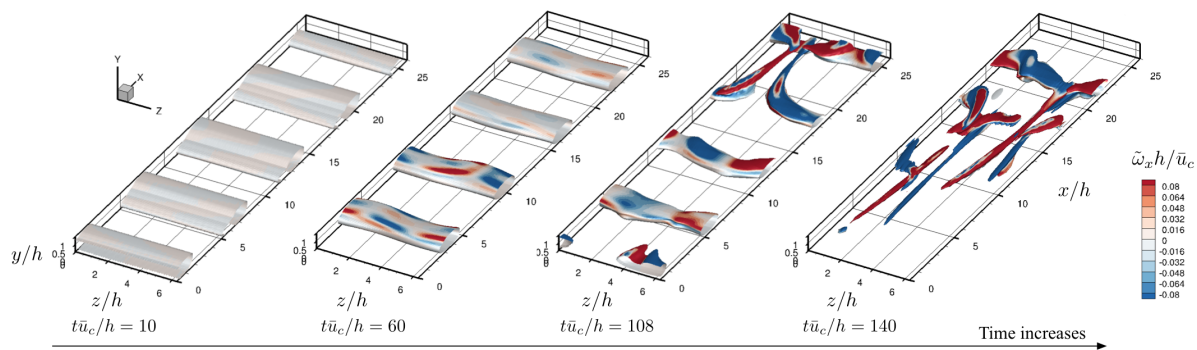


**Fig. 5** Time evolution of flow field to illustrate the laminar-to-turbulent transition process for the case  $(\alpha, \beta) = (1, 0)$ . The flow is initialized by optimal disturbance with kinetic energy density of  $E_0 = 1.0 \times 10^{-4}$ . Iso-surfaces of  $Q$  colored by streamwise vorticity  $\tilde{\omega}_x h / \bar{u}_c$  are visualized. Only the upper half domain ( $y \geq 0$ ) is displayed for clarity.

The transitional process in this case is very similar to the oblique disturbance discussed above in section III.A.1. The transition is directly caused by a break of streamwise streaks that grow from the amplified optimal disturbance. It suggests that the transient energy growth of optimal disturbance solely does not trigger the transition; rather, it is the combined

effect of the growing optimal disturbance and induced secondary instabilities that leads to a laminar-to-turbulent transition. The friction velocity and evolution of transient energy density of disturbance with  $(\alpha, \beta) = (1, 0)$  are shown in figure 6. The features observed from the case  $(\alpha, \beta) = (1, 1)$  also apply on this streamwise-wave disturbance; the flow tends to transition into a turbulent state when the kinetic energy density  $E$  of disturbance is large, which is influenced by both the initial amplitude of the disturbance and corresponding amplification rate.

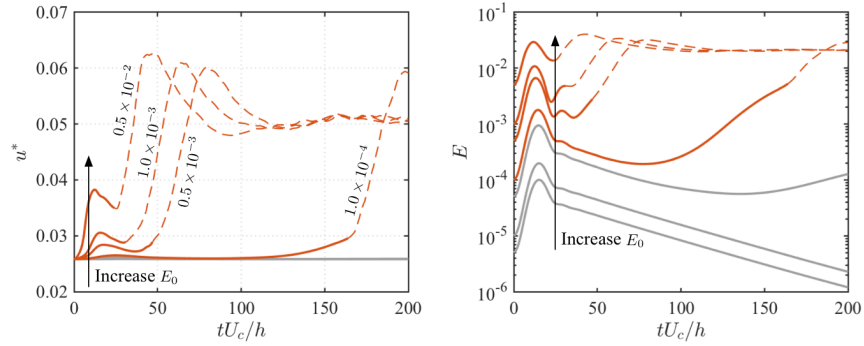


**Fig. 6** Time evolution of friction velocity  $u^*$  (left) and kinetic energy density (right) of case  $(\alpha, \beta) = (1, 0)$  initialized by different amplitudes of optimal disturbance  $E_0$ . Red lines represent transitional cases, and dashed line indicates that the flow is in turbulent state.

### 3. Spanwise-wave disturbance $(\alpha, \beta) = (0, 2)$

The optimal disturbance associated with wavenumber pair of  $(\alpha, \beta) = (0, 2)$  is in form of streamwise vortices. Shown in figure 7 are the flow fields with initial kinetic energy density of  $E_0 = 1.0 \times 10^{-4}$ . When the optimal disturbance grows initially, two co-rotating vortices aligned vertically merge into a large streamwise vortical structure. The structure remains uniform in the streamwise direction, and the corresponding transient energy reaches the maximum value around  $t\bar{u}_c/h = 60$  (as seen in figure 8). After the kinetic energy starts to decrease, the flow gradually experiences spatial variation as seen at  $t\bar{u}_c/h = 150$  that axial rotational motion around the streamwise vortical structures with comparable scale to the streamwise domain length is observed. Next, the kinetic energy density of the flow increases again after  $t\bar{u}_c/h = 150$ , and smaller structures appear in the flow (as seen at  $t\bar{u}_c/h = 240$ ). After a short duration of rotational motion in the flow, a laminar-to-turbulent transition happens around  $t\bar{u}_c/h = 300$ . Based on the features of transient energy growth and corresponding flow fields, we note that the transition is a slow process covering several stages, which cannot be determined simply based on the features of energy growth time histories.

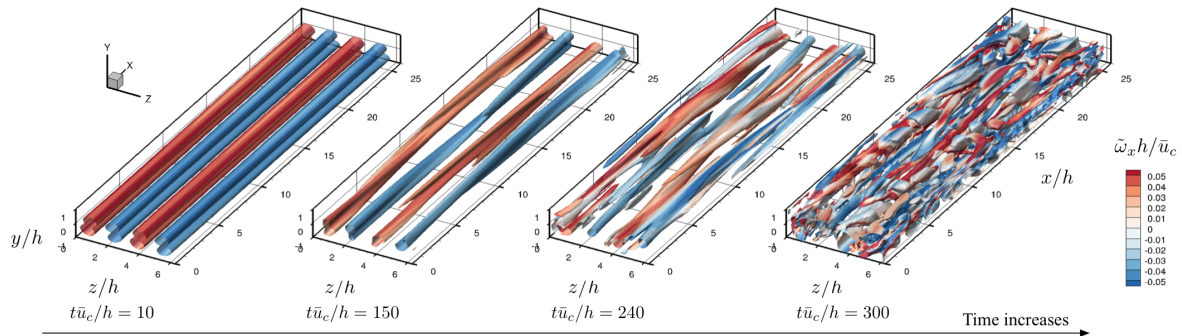


**Fig. 7** Time evolution of flow field to illustrate the laminar-to-turbulent transition process for the case  $(\alpha, \beta) = (0, 2)$ . The flow is initialized by optimal disturbance with kinetic energy density of  $E_0 = 1.0 \times 10^{-4}$ . Iso-surfaces of  $Q$  colored by streamwise vorticity  $\tilde{\omega}_x h / \bar{u}_c$  are visualized.

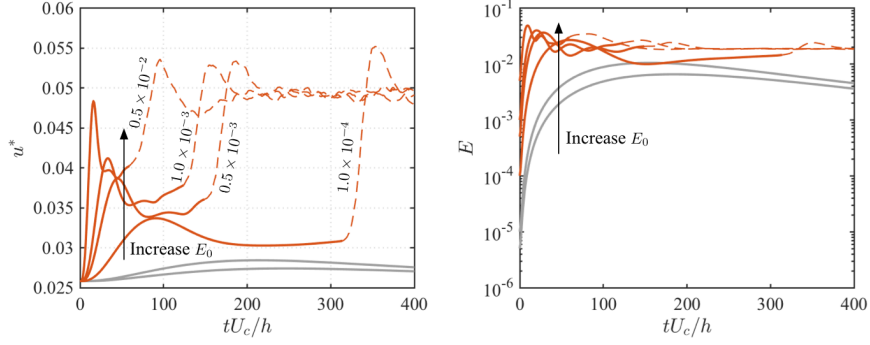


**Fig. 8** Time evolution of friction velocity  $u^*$  (left) and kinetic energy density (right) of case  $(\alpha, \beta) = (0, 2)$  initialized by different amplitudes of optimal disturbance  $E_0$ . Red lines represent transitional cases, and dashed line indicates that the flow is in turbulent state.

### B. Suppression of laminar-to-turbulent transition

In the linear analysis, we synthesized a full-state feedback controller guided by the LQR feedback control law. The transient energy growth is significantly reduced with the corresponding wall actuation, as shown in figure 9. In the nonlinear simulations, we updated the control input  $U$  at each time step using the flow state  $X$  and the gain matrix  $K$  calculated from the linear analysis. Accordingly, the boundary condition of wall-normal velocity  $v_{\pm h}$  is modified based on the control input  $U$ .

To evaluate the overall performance of the controlled flow in terms of reducing large transient energy growth, the optimal disturbance was re-calculated due to a modification of the dynamic system by changing flow boundary conditions from no-slip to blowing/suction actuation. In other words, the optimal disturbance computed based on uncontrolled system might not be the one that is able to lead a maximum transient energy growth in the controlled system. We have also evaluated the amplification of optimal disturbances from both uncontrolled and controlled system in the linear analysis of controlled system, in which the optimal disturbance of the feedback controlled system leads to a higher transient energy growth than the one calculated from the uncontrolled system.

#### 1. Reduction in transient energy growth

Transient energy growth in each controlled case is observed to exhibit similar features as in the uncontrolled cases; namely that an increase in initial kinetic energy makes the amplification of perturbation energy decrease as shown in figure 9. Using case  $(\alpha, \beta) = (1, 0)$  as an example, since the amplification of the optimal disturbance is effectively reduced with the feedback controller, the trajectories of cases with  $E_0 \gtrsim 1.1 \times 10^{-3}$  almost overlap the linear result denoted by red dots. This suggests that, as the growth of the disturbance is suppressed to have small magnitude, the importance of the nonlinearity is weakened. Therefore, the results from nonlinear simulations match the result from linear analysis as the small disturbance assumption is satisfied.

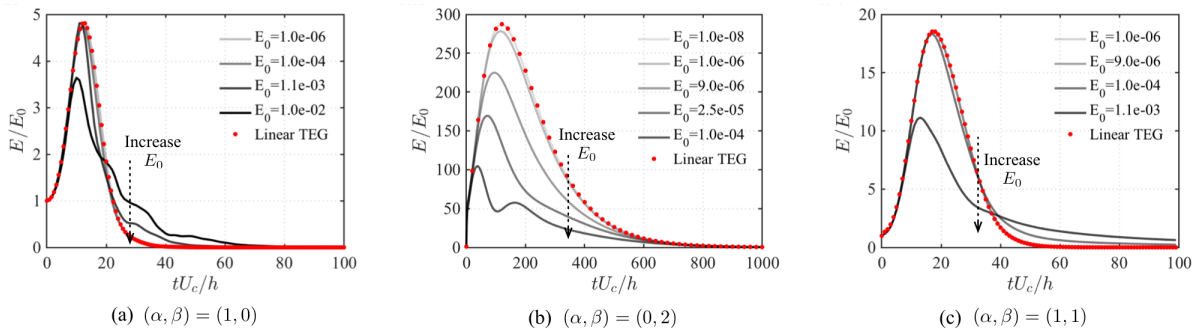


**Fig. 9** Transient energy growth of optimal disturbance with a range of initial kinetic energy density  $E_0$  from linear (red dots) and nonlinear (solid lines) simulations for controlled flows.

For each wavenumber pair, a comparison of the maximum of  $E/E_0$  initiated from a range of optimal disturbance amplitudes is shown in figure 10. For small disturbance amplitude, the percent reduction of maximum transient energy remains almost identical, indicating the nonlinearity of small disturbance is negligible as assumed in the linear analysis. Moreover, each wavenumber scenario reaches the largest reduction of  $\approx 80\%$  in  $(E/E_0)_{\max}$  for small initial amplitude of disturbance. For the case with  $(\alpha, \beta) = (0, 2)$ , this large amount of reduction in  $E/E_0$  only applies to  $E_0 \lesssim O(10^{-5})$ . As the initial disturbance grows in amplitude, the control performance in terms of suppressing the energy amplification degrades, such that the  $(E/E_0)_{\max}$  is nearly unchanged for cases with  $E_0 > O(10^{-3})$ . Similar findings are also observed in the other two disturbance scenarios, but the good reductions in  $(E/E_0)_{\max}$  maintains up to  $E_0 \approx O(10^{-4})$  and  $E_0 \approx O(10^{-3})$  for case  $(\alpha, \beta) = (1, 1)$  and  $(\alpha, \beta) = (1, 0)$ , respectively.

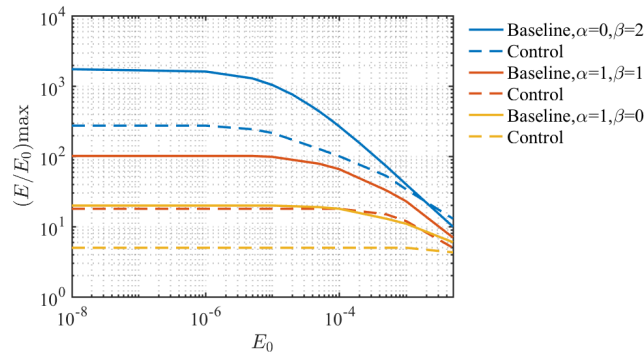


**Fig. 10** A comparison of maximum amplified transient energy density  $(E/E_0)_{\max}$  of a range of amplitude of initial optimal disturbance between uncontrolled (solid lines) and controlled (dashed lines) cases.

## 2. Controlled flow with oblique or streamwise-wave disturbances

By reducing the transient energy growth using the feedback controller, the laminar-to-turbulent transition experienced in the flow with oblique or streamwise-wave disturbances has been successfully suppressed. In other words, the threshold becomes higher in terms of triggering the transitional process. Here, we examine how the wall actuation modifies the flow characteristics to prevent the transition in the uncontrolled flow. Because the control mechanism is similar in the cases with oblique and streamwise-wave disturbances, i.e.,  $(\alpha, \beta) = (1, 1)$  and  $(1, 0)$ , respectively, we will use the flow with oblique disturbance as an example to illustrate the control mechanism.

The transient energy growth present in the uncontrolled flow is caused by a development of large-scale coherent structures, which induces streamwise vortices that further cause a transition to turbulence as discussed above. A comparison of flow features during transitional process between uncontrolled and controlled flows is shown in figure 11. For a fair comparison, here both simulations start from the same optimal disturbance calculated from the uncontrolled flow. In the uncontrolled flow, large magnitude of the initial optimal disturbance is concentrated near the upper and lower walls where coherent structures denoted by  $Q$ -criterion gradually grow into large scale. When the vertical size of the structures increases to almost the half height of the channel, the kinetic energy of perturbation reaches its maximum value around  $t\bar{u}_c/h = 21$ . During this process, streamwise vortices creep in near the walls following the advection of the coherent structures. After  $t\bar{u}_c/h = 21$ , the coherent structures start to decay leaving the induced streamwise vortices in the flow, especially in the vicinity of the channel walls. As these vortices evolve, break and interact with each other, the flow becomes chaotic and a laminar-to-turbulent transition happens. Therefore, the key factor leading to the final transition to turbulence is the breakdown of the streamwise vortices. These streamwise vortices are generated by the rapid growth of the large-scale coherent structures.

Compared to the mechanism observed from the uncontrolled flow, the most apparent change in the flow by introducing wall-normal actuation is the growth of the coherent structures. As shown in figure 11 (right), the actuation on the wall modifies the distribution of high shear in the flow, in which local areas of high shear stress are created and constrained in the vicinity of the channel walls. As a consequence, the growth of the coherent structure is confined near the walls. Because the strength of these relatively small coherent structures is not strong enough to induce high-level of streamwise vortices, the transition observed from the uncontrolled flow is avoided ultimately.

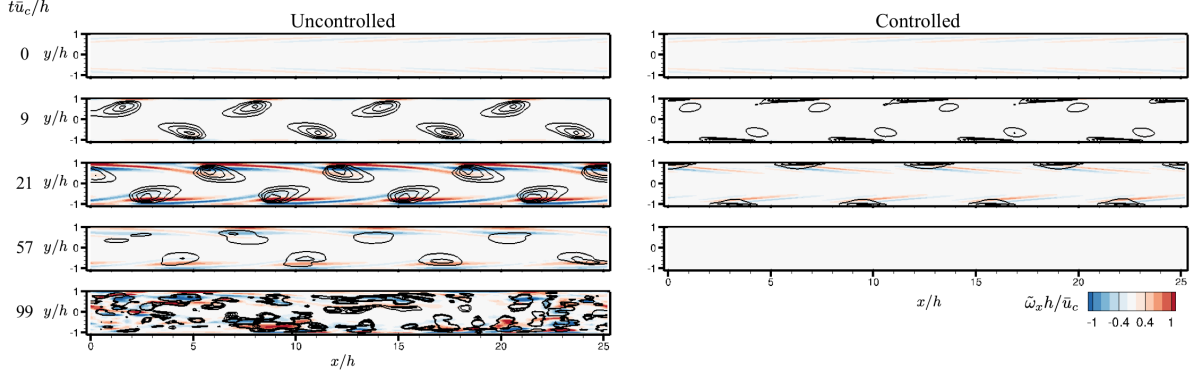


**Fig. 11** A comparison of instantaneous streamwise vorticity  $\tilde{\omega}_x h / \bar{u}_c$  flow fields at slice  $z/h = 0$  between uncontrolled and controlled cases with  $(\alpha, \beta) = (1, 1)$  and  $E_0 = 0.5 \times 10^{-4}$ . Black contour lines denote  $Q$ -criterion in a range of  $0.01 \leq Q(h/\bar{u}_c)^2 \leq 0.05$ .

### 3. Controlled flow of spanwise-wave disturbances

In the transitional process of the flow with spanwise-wave disturbance  $(\alpha, \beta) = (0, 2)$ , the merging process of the two co-rotating vortices makes the base velocity profile highly distorted, as seen in figure 12. The generation of high shear areas introduces secondary instabilities into the flow as discussed above for the uncontrolled flow. To examine the control mechanism, we compare the shear flow fields at  $t\bar{u}_c/h = 50$  when the maximum energy appears between uncontrolled and controlled flow in figure 12. In the uncontrolled flow, high magnitude of shear stress  $\partial u / \partial z$  is formed between the merged vortices horizontally, where we observed the instabilities in figure 7 previously. In the controlled flow, a strong actuation is introduced into the flow, forming small-scale streamwise vortices near walls as denoted in figure 12 (b). The presence of these induced vortices hinders the development of the merged vortices to further grow into large amplitude. Instead, the large streamwise vortical structures are compressed and centralized in the channel. Due to the lack of the well-grown large vortices in the flow, the high shear stress between the vortices are also weakened as revealed by  $\partial u / \partial z$ , providing less chances for the secondary instabilities to creep in.

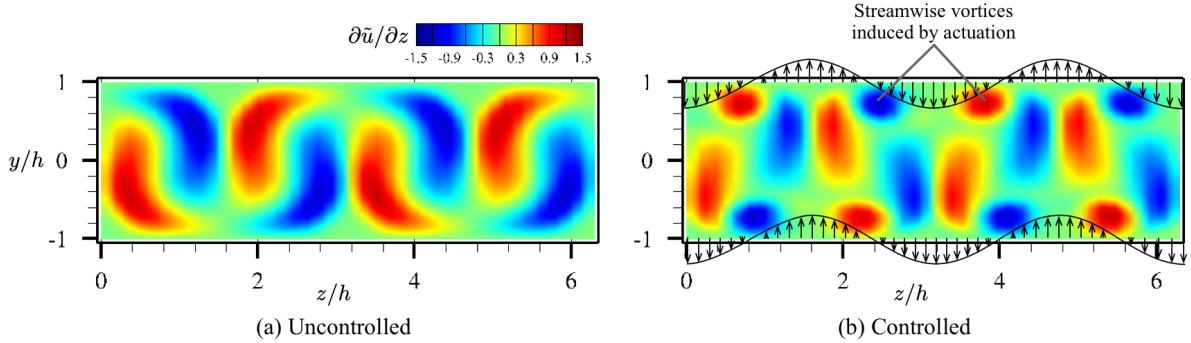


**Fig. 12** Modification of instantaneous streamwise velocity gradient in spanwise direction  $\partial \bar{u} / \partial z$  at slice  $x/h = 0$  and  $t\bar{u}_c/h = 50$  in (b) controlled flow compared to (a) uncontrolled flow. Actuation velocity is denoted by black arrows.

Although the controller has suppressed the growth in large streamwise vortical structures, actually the actuation introduces extra high-shear regions. As shown in figure 13 (a) and (b), the areas denoted by (i) and (ii) indicate induced high-shear stress. Accordingly, as seen in figure 13 (c), new secondary instabilities creep in based on the new high-shear regions of (i) and (ii), which leads to a transition to turbulence ultimately. Hence, though the strengths of the streamwise vortices are suppressed before  $t\bar{u}_c/h = 50$ , as shown in figure 12, the secondary instabilities are introduced by the actuation, which is not accounted for in the controller design from the linear model.

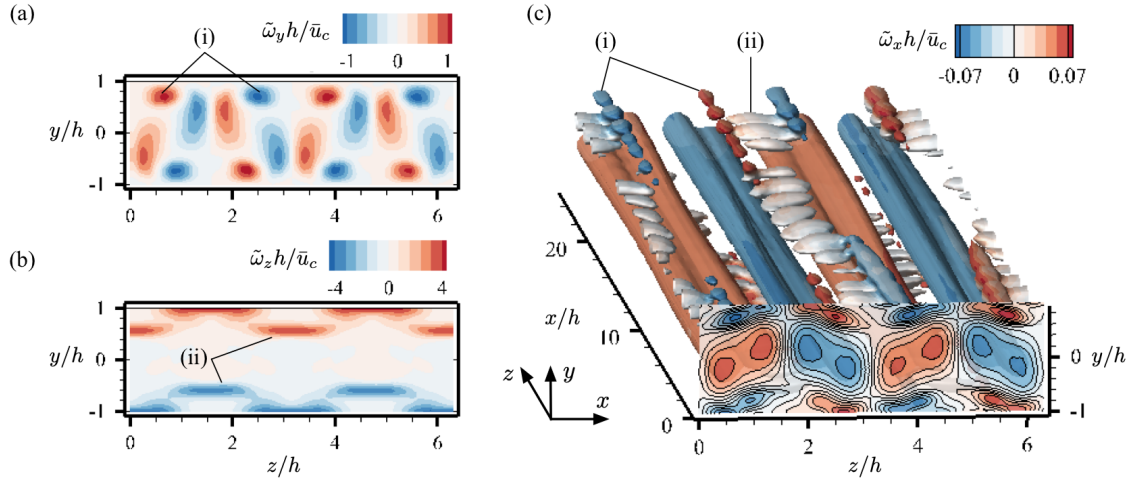


**Fig. 13** Secondary instabilities induced by the actuation in the flow field at  $t\bar{u}_c/h = 66$  of controlled case with  $(\alpha, \beta) = (0, 2)$  and  $E_0 = 1.0 \times 10^{-4}$ . (a) Wall-normal vorticity at slice of  $x/h = 0$ , (b) spanwise vorticity at slice of  $x/h = 0$ , and (c) iso-surfaces of  $Q$  colored by streamwise vorticity.

#### 4. Increase of threshold for laminar-to-turbulent transition

A summary of the cases considered in the present work is provided in figure 14 based on the nonlinear simulation results. For all the three wavenumber pairs, the LQR controller successfully suppresses the transient energy growth from the linear analysis. In the nonlinear simulation that consider the amplitude of the initial optimal disturbance, the threshold for a laminar-to-turbulent transition to appear is increased in the cases of streamwise-wave  $(\alpha, \beta) = (1, 0)$  and oblique  $(\alpha, \beta) = (1, 1)$  disturbances by roughly an order of  $O(10)$  in amplitude. For the spanwise-wave disturbance  $(\alpha, \beta) = (0, 2)$  case, although LQR controller successfully suppresses the transient energy growth of the streamwise coherent structures, new instabilities are induced by the strong actuation applied on the walls, which leads to laminar-to-turbulent transition by another route; hence, the threshold does not change based on the cases considered.

## IV. Conclusion

In this paper, we examine the laminar-to-turbulent transition in plane Poiseuille flow due to a transient energy growth of optimal disturbances at a subcritical Reynolds number of  $Re = 3000$ . Nonlinear effects on transient energy growth are investigated by performing direct numerical simulations. We found that with the presence of nonlinearity in the flow, an increase in initial energy density of optimal disturbance leads to a reduction of amplification rate of the initial disturbance. Moreover, we uncovered the underlying physics of the transitional process for all the disturbances considered. For disturbances associated with  $(\alpha, \beta) = (1, 1)$  and  $(1, 0)$ , the transient energy growth corresponds to the development of large coherent structures. The evolution of these large-scale coherent structures induces a growth of streamwise vortices near channel walls, and the breakdown of these vortices leads to a laminar-to-turbulent transition. For disturbance associated with  $(\alpha, \beta) = (0, 2)$ , the base flow is highly distorted due to the growth of streamwise vortices, which results in high-shear-stress regions formed between the streamwise vortical structures. These high-shear areas introduce secondary instabilities that lead to a laminar-to-turbulent transition.

Feedback controllers are designed using linear quadratic regulator, which have been shown capable of reducing transition energy growth via wall-normal blowing and suction actuation at the upper and lower walls. In the controlled flow initiated from streamwise-wave  $(\alpha, \beta) = (1, 0)$  and oblique  $(1, 1)$  disturbances, the wall actuation modifies the shear distribution in the flow such that coherent structures can only form in the vicinity of the channel walls and decays earlier than the uncontrolled flow. Laminar-to-turbulent transition is prevented because the hindered growth of coherent structures significantly inhibits the strength of induced streamwise vortices. The control strategy can increase the threshold for transition by approximately  $O(10)$  in magnitude. For the case with spanwise-wave disturbance of  $(\alpha, \beta) = (0, 2)$ , the controller has not effectively increased the threshold for the transition since the actuation induces extra instabilities that lead the flow to transition from a laminar to turbulent state. The present work has shown the capability of feedback control for suppressing transient energy growth and preventing laminar-to-turbulent transition.

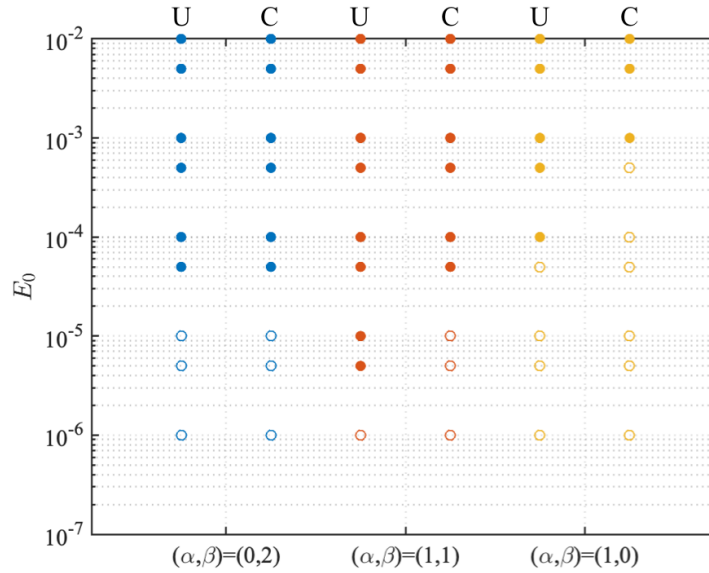


**Fig. 14** Summary of cases considered in the present work. Solid circle represents transitional case, and open circle denote case that a laminar-to-turbulent transition does not happen. U and C denote uncontrolled and controlled cases, respectively.

The nonlinear effects and underlying physics related to transitional process have been investigated by performing direct number simulations. The findings obtained from this study can offer valuable insights into the physical-mechanism that enable transition delay by feedback control. These insights can provide guidance on actuation strategies for future investigations.

### Acknowledgments

This material is based upon work supported by the Air Force of Scientific Research under award numbers FA9550-17-1-0252 and FA9550-19-1-0034. We thank Minnesota Supercomputing Institute for providing computational resources.

### Appendix

#### References

- [1] Stuart, J. T., "On the non-linear mechanics of wave disturbances in stable and unstable parallel flows Part 1. The basic behaviour in plane Poiseuille flow," *J. Fluid Mech.*, Vol. 9, 1960, pp. 353–370.
- [2] Watson, J., "On the non-linear mechanics of wave disturbances in stable and unstable parallel flows Part 2. The development of a solution for plane Poiseuille flow and for plane Couette flow," *J. Fluid Mech.*, Vol. 9, 1960, pp. 371–389.
- [3] Nishioka, M., A. S. I., and Ichikawa, Y., "An experimental investigation of the stability of plane Poiseuille flow," *J. Fluid Mech.*, Vol. 72, 1975, pp. 731–751.
- [4] Henningson, D. S., and Kim, J., "On turbulent spots in plane Poiseuille flow," *J. Fluid Mech.*, Vol. 228, 1991, pp. 183–205.
- [5] Elofsson, P. A., Kawakami, M., and Alfredsson, P. H., "Experiments on the stability of streamwise streaks in plane Poiseuille flow," *Phys. Fluids*, Vol. 11, No. 915, 1999.
- [6] Thomas, L. H., "The stability of plane Poiseuille flow," *Phys. Rev.*, Vol. 91, No. 780, 1953.
- [7] Orszag, S. A., "Accurate solution of the Orr-Sommerfeld stability equation," *J. Fluid Mech.*, Vol. 50, 1971, pp. 689–703.

- [8] Gustavsson, L. H., “Energy growth of three-dimensional disturbances in plane Poiseuille flow,” *J. Fluid Mech.*, Vol. 224, 1991, pp. 241–260.
- [9] Schmid, P. J., and Henningson, D. S., *Stability and transition in shear flows*, Springer, 2001.
- [10] Orszag, S. A., and Kells, L. C., “Transition to turbulence in plane Poiseuille and plane Couette flow,” *J. Fluid Mech.*, Vol. 96, 1980, pp. 159–205.
- [11] Nishioka, M., and Asai, M., “Some observations of the subcritical transition in plane Poiseuille flow,” *J. Fluid Mech.*, Vol. 150, 1985, pp. 441–450.
- [12] Chapman, S. J., “Subcritical transition in channel flows,” *J. Fluid Mech.*, Vol. 451, 2002, pp. 35–97.
- [13] Schmid, P. J., “Nonmodal Stability Theory,” *Annu. Rev. Fluid Mech.*, Vol. 39, 2007, pp. 129–162.
- [14] Hanifi, A., Schmid, P. J., and Henningson, D. S., “Transient growth in compressible boundary layer flow,” *Phys. Fluids*, Vol. 8, No. 826, 1996.
- [15] Joshi, S. S., Speyer, J. L., and Kim, J., “A systems theory approach to the feedback stabilization of infinitesimal and finite-amplitude disturbances in plane Poiseuille flow,” *J. Fluid Mech.*, Vol. 332, 1997, pp. 157–184.
- [16] Bewley, T. R., and Liu, S., “Optimal and robust control and estimation of linear paths to transition,” *J. Fluid Mech.*, Vol. 365, 1998, pp. 305–349.
- [17] Hogberg, M., Bewley, T. R., and Henningson, D., “Linear feedback control and estimation of transition in plane channel flow,” *J. Fluid Mech.*, Vol. 481, 2003, pp. 149–175.
- [18] Kim, J., and Bewley, T. R., “A linear systems approach to flow control,” *Annu. Rev. Fluid Mech.*, Vol. 39, 2007, pp. 383–417.
- [19] Ilak, M., and Rowley, C. W., “Feedback control of transitional channel flow using balanced proper orthogonal decomposition,” AIAA Paper 2008-4230, 2008.
- [20] Martinelli, F., Quadrio, M., McKernan, J., and Whidborne, J. F., “Linear feedback control of transient energy growth and control performance limitations in subcritical plane Poiseuille flow,” *Phys. Fluids*, Vol. 23, 2011.
- [21] Jones, B. L., Heins, P. H., Kerrigan, E. C., Morrison, J. F., and Sharma, A. S., “Modelling for robust feedback control of fluid flows,” *J. Fluid Mech.*, Vol. 769, 2015, pp. 687–722.
- [22] Heins, P. H., Jones, B. L., and Sharma, A. S., “Passivity-based output-feedback control of turbulent channel flow,” *Automatica*, Vol. 69, 2016, pp. 348–355.
- [23] Whidborne, J. F., and Amar, N., “Computing the maximum transient energy growth,” *BIT Numerical Mathematics*, Vol. 51, 2011, pp. 447–457.
- [24] Kerswell, R. R., “Nonlinear Nonmodal Stability Theory,” *Annu. Rev. Fluid Mech.*, Vol. 50, 2018, pp. 319–345.
- [25] Hemati, M. S., and Yao, H., “Performance limitation of observer-based feedback for transient energy growth suppression,” *AIAA J.*, Vol. 56, No. 6, 2018.
- [26] Yao, H., and Hemati, M. S., “Revisiting the separation principle of improved transition control,” AIAA Paper 2018-3693, 2018.
- [27] Kalur, A., and Hemati, M. S., “Reduced-order models for feedback control of transient energy growth,” AIAA Paper 2018-3690, 2018.
- [28] Yao, H., and Hemati, M. S., “Advances in output feedback control of transient energy growth in a linearized channel flow,” AIAA Paper 2019-0882, 2019.
- [29] McKernan, J., Papadakis, G., and Whidborne, J. F., “A linear state-space representation of plane Poiseuille flow for control design - a tutorial,” *International J. of Modeling, Identification and Control*, Vol. 1, No. 4, 2006, pp. 272–280.
- [30] Brogan, W. L., *Modern Control Theory*, Pearson, 1991.
- [31] Gibson, J. F., “Channelflow: A spectral Navier-Stokes simulator in C++,” Tech. rep., U. New Hampshire, 2014. [Channelflow.org](http://Channelflow.org).

- [32] Gibson, J. F., Halcrow, J., and Cvitanović, P., “Visualizing the geometry of state space in plane Couette flow,” *J. Fluid Mech.*, Vol. 611, 2008, pp. 107–130. [arXiv:0705.3957](https://arxiv.org/abs/0705.3957).
- [33] Reddy, S. C., Schmid, P. J., Baggett, J. S., and Henningson, D. S., “On stability of streamwise streaks and transition thresholds in plane channel flows,” *J. Fluid Mech.*, Vol. 365, 1998, pp. 269–303.
- [34] Hunt, J. C. R., Wray, A. A., and Moin, P., “Eddies, streams, and convergence zones in turbulent flows,” *Proc. of the Summer Program, Center of Turbulence Research*, 1988, pp. 193–208.